The effect of groove texture patterns on piston-ring pack friction

S. Mezghani [a], I. Demirci [a,*], H. Zahouani [b], M. El Mansori [a]

[a] Arts et Métiers Paristech, LMPF, Rue Saint Dominique, BP 508, 51006 Châlons en Champagne, France
[b] Laboratoire de Tribologie et Dynamique des Systèmes, UMR CNRS 5513, Ecole Centrale de Lyon, 36 avenue Guy de Collongue, 69131 Ecully Cedex, France

Keywords:
Surface texture
Honing
Hydrodynamic friction

A B S T R A C T

A cylinder liner possesses fairly intricate surface requirements due to its complicated functions. It needs to provide adequate surface roughness to resist wear as well as to store and retain lubricants during high temperatures. The liner surface texture is anisotropic, produced by the honing process, with resultant deep visible scratches left on it [1]. The prominence of the honing grooves observed suggests that surface texture significantly affects ring-pack performance, although this effect is not clearly understood.

In this paper, a numerical model was developed to investigate the effects of groove characteristics on the lubrication condition and friction at the interface between the piston ring and cylinder liner. This model aims to solve the average Reynolds equation, which depends on the real surface topographies of the cylinder liner, and describes the influence of surface irregularities on the lubricant flow under hydrodynamic lubrication conditions, considering lubricant film rupture and cavitations. Numerical results help to determine the optimum lateral groove characteristics to reduce friction and then noxious emissions.

1. Introduction

Increasingly stringent engine-emission standards and power requirements are driving an evolution in cylinder liner surface finish [1]. The final surface finish on the cylinder bore however, is created by the honing process. Honing is designed to create a controlled surface finish on the cylinder liner [2]. The cylinder bore texture mainly consists of two sets of straight, approximately parallel grooves placed stochastically and appearing at different angles to the cylinder axis [3,4]. The angle between the honing grooves perpendicular to the cylinder axis is termed the cross-hatch angle. A typical honed surface texture from an engine cylinder is shown in Fig. 1.

The honed surface texture can be divided into two principal components: plateaus and valleys with depths that are greater than the surface roughness [4]. The plateau component is related to friction and wear. In fact, the coefficient of friction in the piston–ring-liner interfaces was proved to increase with the average roughness of the surface liner [2,5]. The valley component is associated with lubricant circulation and reservoirs. Their prominence suggests a significant role in the effect of surface texture on ring-pack performance [2].

Understanding and optimizing the surface texture, such as liner surface finish, have become the focus of researchers and engineers to meet the requirements of engine performance and durability in the future [2,6]. Traditionally, deterministic models or expensive experimental tests are used to solve these issues. Reciprocating bench test has been applied in several experimental studies, to identify the effect of some surface patterns (roughness, cross-hatch angle, laser texturing, . . .) [7–12].

Besides, friction is an important factor to be considered when sliding surfaces at high contact pressures are involved. A majority portion of these friction losses is determined by the piston/piston ring/running surface module. Friction reduction is highly desirable as it reduces fuel consumption. Some experimental studies demonstrate that the reduction of liner roughness has the strongest effect on reducing the ring-pack friction [2,12]. Therefore, ring-pack roughness should also be reduced, if possible. However, such an approach cannot separately and rigorously identify the effect of each surface feature. Therefore, the full effect of different cylinder liner finishes on ring-pack performance is still not well understood. A numerical optimization approach of the cylinder liner surface thus becomes inevitable. Several numerical models were developed over recent years to simulate the piston ring-pack contact [13–16].

This paper aims to investigate the effects of groove texture of cylinder liner surface on ring-pack friction, mainly to reduce friction loss without prejudice to the oil consumption. But, oil consumption is practically impossible to determine numerically so only friction performance is considered in this work. A numerical model considering the 3D liner surface texture has been developed to study the lateral grooves characteristics effect on friction. It predicts the friction of piston ring cylinder liner contact in purely hydrodynamic regime. At the end of the successive honing stage,

* Corresponding author. Tel.: +33 0 3 26 69 91 35; fax: +33 0 3 26 69 91 76.
E-mail address: Ibrahim.demirci@ensam.fr (I. Demirci).

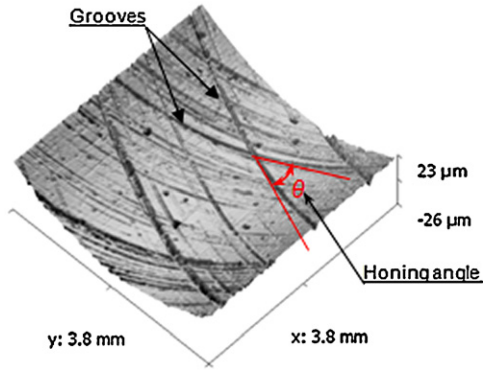

Fig. 1. Plateau honed surface of thermal engine cylinder.

the plateau roughness is very low comparatively to grooves height. Then, in all this study, the plateau of honed surface texture is assumed smooth.

2. Numerical model description

A numerical model was developed to estimate the friction in the ring-liner–piston contact, considering the real topography of the cylinder liner. The objective of this model is to qualitatively predict the friction coefficient obtained using different groove characteristics of cylinder liner surfaces to optimize their performances.

2.1. Geometry definition

An incompressible viscous fluid occupying, at a given moment, a field limited by a smooth plane surface *P* and by a rough surface *R*, is considered. This field is represented in Fig. 2 (we did not represent the profile in the x_2 direction). It extends from 0 to l_1, 0 to l_2 and $h\ (x_1, x_2)$ respectively, according to x_1, x_2 and x_3. The "h" (x_1, x_2) represents the fluid thickness. The smooth body is animated by movement at a constant velocity "u_1" along the Ox_1 axis, whereas the rough surface is static.

2.2. Equation

To simulate the hydrodynamic contact, the famous Reynolds equation derived from the Navier–Stokes equation for slow viscous flow (both inertia and external forces are neglected with respect to viscous forces) is used. Another simplification is due to the dimension in the x_3 direction, which is much smaller than those in x_1 and

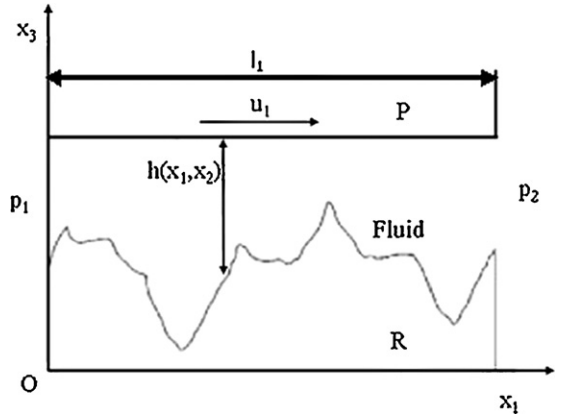

Fig. 2. The separation field between a smooth surface and a rough one.

x_2 directions. An average of this equation is often incorporated for the tribological studies in the hydrodynamic contacts.

The Reynolds equation, in two dimensions, is given by:

$$\frac{\partial}{\partial x_1}\left(\frac{\rho h^3}{\mu}\frac{\partial p}{\partial x_1}\right)+\frac{\partial}{\partial x_2}\left(\frac{\rho h^3}{\mu}\frac{\partial p}{\partial x_2}\right)=6u_1\frac{\partial \rho h}{\partial x_1} \tag{1}$$

where h is the film thickness, p is the pressure, μ is the viscosity, ρ is the fluid density and u_1 the smooth body velocity. The fluid is considered isoviscous. These equations will be used in dimensionless form. The pressure field is non-dimensional by atmospheric pressure p_0. A characteristic length, h_m, was defined to normalize the lengths of the problem corresponding to the average fluid film thickness. The new dimensionless variables are:

$$P=\frac{p}{p_0};\qquad X_1=\frac{x_1}{h_m};\qquad X_2=\frac{x_2}{h_m};\qquad H=\frac{h}{h_m} \tag{2}$$

In this manner, the Reynolds equation is expressed by:

$$\frac{\partial}{\partial X_1}\left(H^3\frac{\partial P}{\partial X_1}\right)+\frac{\partial}{\partial X_2}\left(H^3\frac{\partial P}{\partial X_2}\right)=\lambda\frac{\partial H}{\partial X_1} \tag{3}$$

with λ termed the *Bearing Number* as a constant and it is equal to $(6\,\mu\,u_1)/h_m p_0$.

To fully solve these equations, several boundary conditions are necessary. The total adhesion of the fluid on the surfaces of the solids is assumed. Further, these conditions are completed by pressures imposed on the front and back faces of the segment:

$$\begin{cases} p(0,x_2)=p_1 \\ p(l_1,x_2)=p_2 \end{cases} \tag{4}$$

Periodic or restrictive Dirichlet conditions were used along the x_2 axis.

Moreover, since the lubricant is assumed to be fluid, pressures lower than the vapour pressure are physically impossible. The fluid will cavitate and the pressure remains constant. This effect is not accounted in the Reynolds equation presented above. On the contrary, in such region the equation will allow pressure to decrease without limit and may predict large negative pressures. The occurrence of cavitation is considered separately. Since in most situations the vapour pressure of the lubricant is of a same order of magnitude as the ambient pressure which is very small compared to the contact pressure. Therefore, the condition is imposed that the pressure should be larger than or equal to zero. This condition lead to a complementary problem and the determining of the exact location of this boundary is a free boundary problem since the pressure distribution is not known. This free boundary is often treated by the Reynolds' cavitation boundary condition:

$$\begin{cases} p=p_{cav} \\ \dfrac{\partial p}{\partial n}=0 \end{cases} \tag{5}$$

where p_{cav} is the saturating steam pressure, generally assumed as atmospheric pressure and n is the outward normal vector to the outlet boundary of the contact also called cavitation boundary. In practice, this condition is obtained on the free surface by setting all negative pressures to zero.

2.3. Galerkin's formulation and numerical procedure

Using Eq. (3), the weak form of the Reynolds equation can be expressed by the following relation:

$$\int_\Omega -\nabla P\nabla\psi\ dX_1\,dX_2+\int_{d\Omega}\nabla P\vec{n}\psi\,dL-\int_\Omega\lambda\frac{\partial H}{\partial X_1}\psi\,dX_1\,dX_2 \tag{6}$$

where the test pressure function ψ is regular and $\psi=0$ on the field borders.

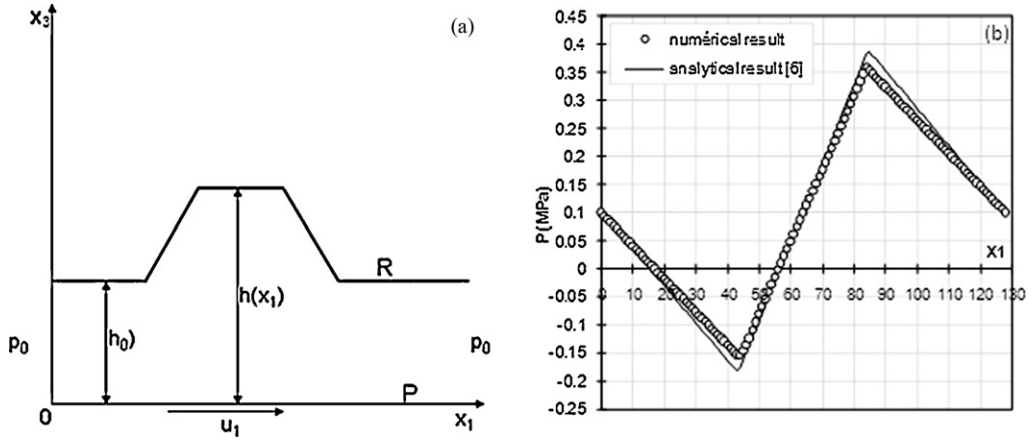

Fig. 3. (a) Validation geometry: trapezoidal profile, (b) numerical and analytical pressure fields obtained for trapezoidal profile.

The traditional finite element method was applied to Eq. (6). This equation coupled with the boundary conditions result in a pressure field on the Ω domain. With this pressure field, it is possible to determine the friction coefficient, which is calculated using the following relation [17]:

$$f_{cx,i} = \frac{\int_{\Omega} \tau_{x_1 x_2,i}\, d\Omega}{w}, \quad i = 1 \quad or \quad 2 \tag{7}$$

where $\tau_{xy,i}$ is evaluated using this following analytic expression:

$$\tau_{x_1 x_2,i} = \mu \dot{\gamma}_{x_1 x_2,i} \tag{8}$$

with $\dot{\gamma}_{x_1 x_2,i} = (1/2\mu)(\partial p/\partial x_1)(2x_3 - h) + ((u_1 - u_2)/h)$where $i = 1$ and corresponds to the smooth body; and $i = 2$ to the rough body' u_1 and u_2 correspond respectively, to the smooth and rough bodies' velocities ($u_2 = 0$).

2.4. Numerical model validation

To validate the model developed, the contact between a plane and the simple geometry including the trapezoidal profile is considered (Fig. 3). This profile includes an elementary pattern of the honed motifs. In fact, the honed surface model based on the bearing area linearization method [3] can be obtained by a series of trapezoidal motifs. This trapezoidal profile varies along the x_1 axis and is invariant following the x_2 axis. The parameters are listed in Table 1, and the analytical solution of contact is given in Caciu [15,16].

Fig. 3(b), which presents the pressure field as a function of the position, shows good correlation between the pressure profile obtained with the developed model and the analytical one. In this validation example, the free boundary has not been considered. This result in negative pressure as observed in Fig. 3(b).

2.5. Application to the ring liner contact

Our aim here is to apply the model developed to the geometry, as shown in Fig. 4. The effect of the liner surface texture is assumed to dominate that of the ring surface texture; therefore, the ring can be approximated by a smooth surface in the flow simulation. This appears reasonable in most cases because the ring surface is typically much smoother than the liner's, with no deep characteristic grooves [2]. A diagram showing the typical layout of a ring cross-section used in simulation is seen in Fig. 4.

The ring and the liner are separated by lubricant thickness h, taking the ring curvature into account. Thus, the oil film thickness can be expressed as:

$$h(x_1, x_2) = h_0 + \frac{x_1^2}{2Rx_1} + \frac{x_2^2}{2Rx_2} + Rh(x_1, x_2) \tag{9}$$

where Rx_1 and Rx_2 are the radius of curvature in x_1 and x_2 directions, respectively, and $Rh(x_1,x_2)$ is the surface amplitude in the position coordinate (x_1,x_2) and h_0 is a constant characterizing the separation of the two body surfaces.

The model developed is a predictive tool, applied to the ring liner contact, to give a representative and qualitative estimation of friction loss for a given groove surface texture. This model considers the dominant mode of lubrication, i.e. hydrodynamic lubrication regime. This regime is effective in the major part of the stroke length and typically present during mid-stroke conditions when there is sufficient lubrication, and sliding speeds are relatively high [18].

For all the numerical simulations, a constant viscosity of $\mu = 0.04$ Pa s, a value typical of mineral oil is considered. The atmospheric pressure is used as a boundary condition ($p_1 = p_2 = p_0$). Velocity varies from 2 to 52 m s^{-1} during numerical simulation.

The real topography of the cylinder liner surface is necessary to solve the Reynolds equation. Fig. 5a shows the 3D topography of the cylinder liner surface using the 3D interferometer (WYKO NT3300). Beginning from this real topography, the oil film thickness (Fig. 5b) is calculated by Eq. (9) and used in the Reynolds equation to determine the pressure field. Using the pressure field and fluid properties, the normal and tangential forces exerted by the fluid and the coefficient of friction are calculated. Then, the

Table 1
Parameters used for the validation of the model.

Parameter	Value
u_1	10 m s^{-1}
p_0	1.013×10^5 Pa
(	900 kg m^{-3}
υ	6×10^{-6} m^2 s
l_1	384.0 μm
l_2	384.0 μm
l_3	3.0 μm

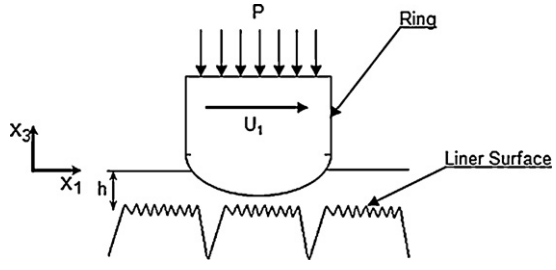

Fig. 4. Piston–liner contact description.

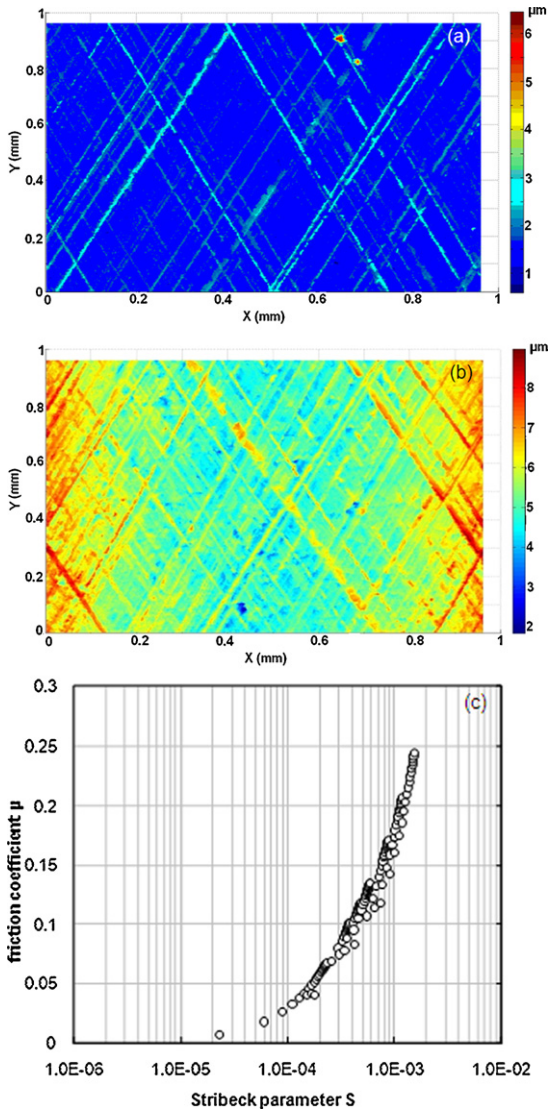

Fig. 5. (a) Honed surface topography, (b) the oil film thickness, and (c) Stribeck curves of the honed surface.

Stribeck curve which indicates the evolution of the friction coefficient versus the Stribeck parameter $S = (\mu \cdot u_1)/p$ is plotted (Fig. 5c). This figure shows that the hydrodynamic regime holds, with chosen microscopic contact parameters (velocity, viscosity, h_0, ...) used in the numerical simulation. The parameters used are listed in Table 2. It is notable that this regime is the predominant one in the piston ring cylinder contact.

Table 2
Parameters used during simulation.

Parameter	Value
u_1	2–52 m s^{-1}
p_0	1.013×10^5 Pa
(	900 kg m^{-3}
μ	0.04 Pa s
l_1	384.0 μm
l_2	384.0 μm
h_0	1.0 μm

3. Numerical simulation of the lateral groove characteristics effect on friction

The valleys play an important role in the functioning of the honed plateau surface as they act as reservoirs of lubrication. To isolate the effect of the lateral groove texture on ring-pack friction, a program was developed using MATLAB software to generate a simulated three-dimensional honed surfaces with different lateral groove patterns. One needs to specify the balance of the grooves R_g, their width L_g and density D_g and the honing cross-hatch angle θ.

3.1. Groove texture characterization

In this study, the Radon transform is used to quantify these features. The very strong feature of this transform is its ability to extract lines from noise images of the honed surfaces. It transforms two-dimensional images with lines into a domain of possible line parameters, where each line in the image will produce a peak, positioned at the corresponding line parameters (amplitude and angle). The Radon transform for a set of parameters (ρ, θ) is the line integral through the image $f(x,y)$, where the line is positioned corresponding to the value of (ρ, θ). The following formula gives the Radon transform [19–21]:

$$TR(\rho, \theta) = \int_{-\infty}^{+\infty} \int_{-\infty}^{+\infty} f(x, y)\delta(\rho - x \cos\theta - y \sin\theta)\, dx\, dy \qquad (10)$$

where δ is the Dirac function.

Fig. 6 shows an application of this transform to a typical honed surface. This description helps to determine the number of straights in the two directions of honed surface grooves. They are obtained by detecting the local maxima in the two directions by radon transform representation (Fig. 6).

Thus, the honing angle, the density and the ratio of the grooves can be objectively determined from this spatial description. The groove density parameter, D_g characterizes the number of grooves by a surface unit according to the following expression:

$$D_g = \frac{N_R + N_L}{S_{area}} \qquad (11)$$

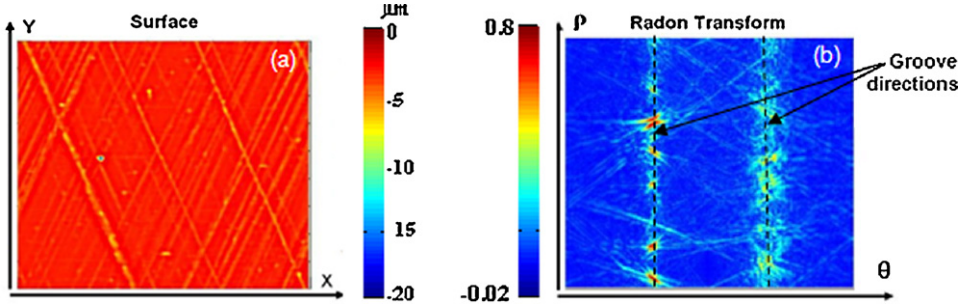

Fig. 6. Plateau honed surface (a) and its radon transform (b).

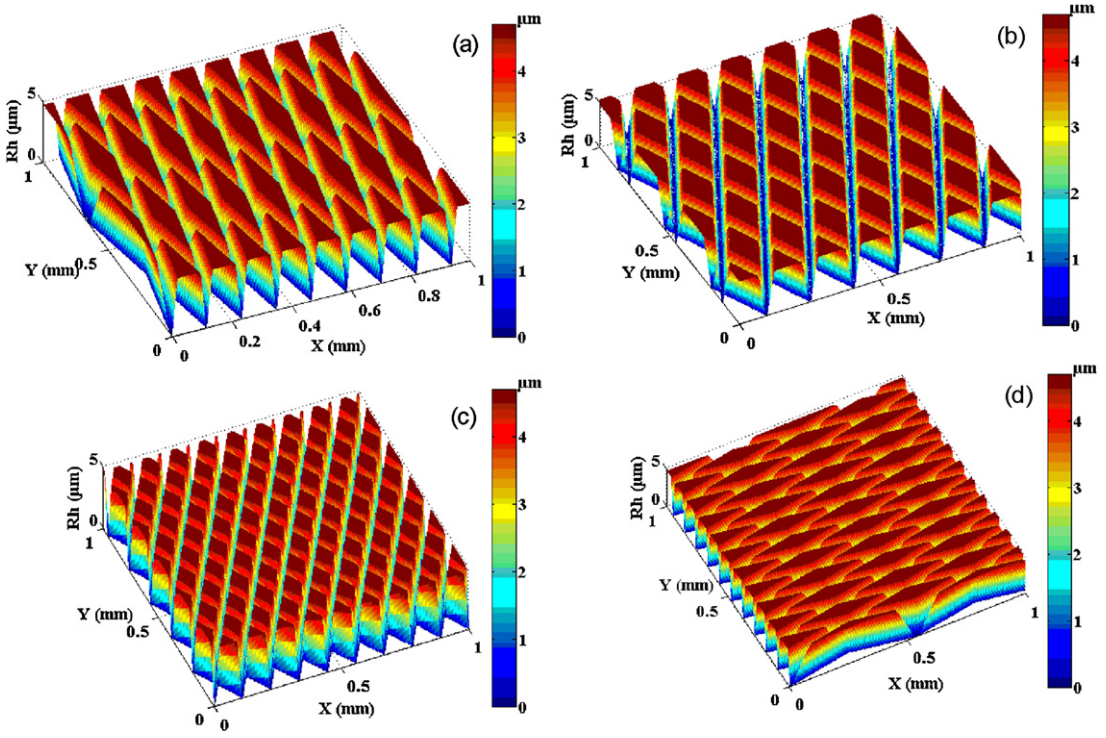

Fig. 7. Simulated honed surface with different honing angles: (a) 20°, (b) 50°, (c) 120° and, (d) 160°.

where N_L and N_R are respectively, the number of grooves in the left and right directions, and S_{area} is the analyzed honed surface area.

The groove ratio parameter R_g reveals the balance of the grooves and defines the ratio of left N_L and right grooves N_R (Eq. (12)):

$$R_g = \frac{Sup(N_R, N_L)}{N_R + N_L} \tag{12}$$

R_g equal to 0.5 shows perfect balanced grooves on the surface texture. When $R_g \to 1$, the texture tends toward a unidirectional surface.

3.2. Effect of honing cross-hatch angle

The honing cross-hatch angles are determined in the actual honing process revealed by the honing stone as it spirals down the cylinder liner, which itself is determined by the feed, and speed rates of the honing tool, with respect to the following formula:

$$\tan\left(\frac{\theta}{2}\right) = \frac{V_a}{V_r} \tag{13}$$

where V_a is the axial speed and V_r is the rotation speed.

Experts opine that the honing angle is directly related to oil consumption and noxious emissions. Scientific studies and practical application have actually shown that oil consumption can be reduced by increasing the honing angle [5]. However, the effect of this geometric property on friction has not been studied earlier because the groove patterns are always associated with lubricant performances. Accordingly, a three-dimensional surface generator was used to simulate surfaces with different honing cross-hatch angles to study the effect of this parameter on the friction behavior of the cylinder ring contact (Fig. 7).

The height of grooves is considered here is equal to 5 µm because real honed surfaces present height varying practically from 3 to 10 µm depending on the honing process conditions.

The coefficient of friction between the piston ring and the cylinder liner is predicted using the model described above. It reflects the energy consumption of the oscillating components, indicates the probability of wear of the sliding surfaces, and reflects the lubrication conditions at the respective positions of the piston.

Fig. 8 shows the influence of the honing angle on the friction coefficient with maintaining statistically identical surface height distributions for all the surfaces generated. By examining Fig. 8, the two minima of friction respectively can be observed for a honing cross-hatch angle range of [40–55°] and [115–130°]. These two honing angle ranges are commonly used in two kinds of honing respectively, plateau honing and helical slide honing. The minimum observed in the second range is in accordance with the experimental test results given in [22]. The 140° honed liners are shown to have the same performance in wear and friction properties for the top dead center area compared to the 40° honing angle.

Some experimental studies reveal that oil consumption is reduced by increasing the honing angle [4,22]. Further, decreasing the honing cross-hatch angle slightly was experimentally shown to

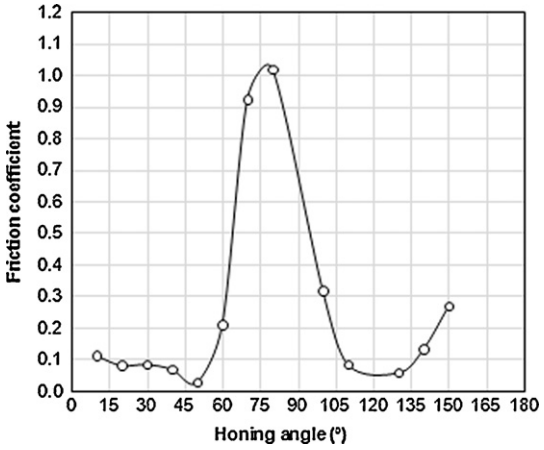

Fig. 8. Effect of honing angle on friction coefficient.

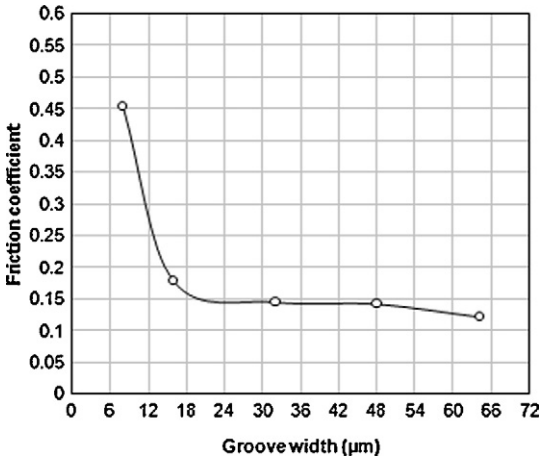

Fig. 9. Friction coefficient vs groove width for contact speed of 20 m s^{-1}.

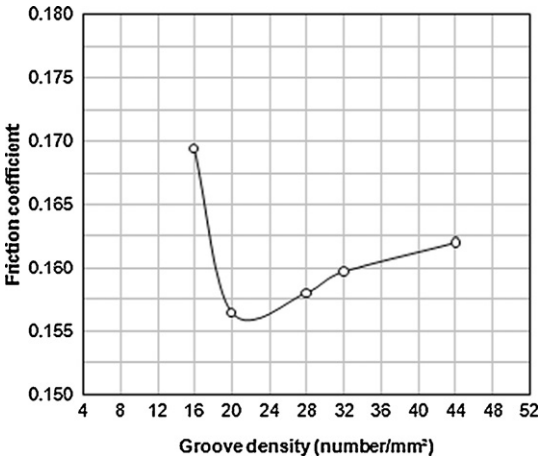

Fig. 10. Friction coefficient vs groove density.

raise the chances of scuffing failure [2]. Therefore, in conclusion it is noted that the helical-slide honing [115–130°] could be the optimized honing process, providing the best global compromise for global engine performance. To study the effect of the other groove features, the honing angle is fixed at 50°.

3.3. Effect of groove width

The honed surfaces are obtained by a succession of three honing stages: the first stage, often categorized as rough honing, establishes the cylindricity of the bore. The second stage or "finish honing" creates the basic surface texture of the hole (valley groove). This enables the third honing operation – plateau stage – to remove the plateau surface peaks, increasing the micro-relief quality without surface damage [23,24].

In this simulation, surface texture with valley width variant from 8 to 64 μm was considered. In fact, the width of valley grooves on honed surface textures produced in automotive industry present width variant from 15 to 35 μm. Moreover, Sabri et al. [20] proved by using a multiscale characterization based on continuous wavelet transform decomposition that the plateau honing affects only wavelengths lower than 20 μm. So valley groove have a widths higher than this limit. Fig. 9 shows the prediction result of friction of the ring cylinder contact for various valley groove widths. For groove width higher than 20 μm, the friction is optimal and remains constant. This result involves that the width of valley grooves has no effect on the friction coefficient. This allows to make link between the process variable and the honed surface functionality (friction performance). In fact, the process can be optimized according to the surface performance. In this context, the grit size and the contact pressure used during finish honing has no impact on the friction performance.

In the following study, the groove width is fixed at 32 μm.

3.4. Effect of groove density

The groove density parameter D_g (Eq. (11)) was determined for various plateau-honed surfaces derived from the honing production series. The conformity of these surfaces is systematically given by the expert's visual inspection. Groove density is known to vary in the range of 20–40 grooves/mm^2. To isolate the effect of plateau roughness variability when comparing the honed surfaces with different groove densities, different groove textures were simulated with groove density variants from 16 to 42 grooves/mm^2. The influence of groove density on friction performance is shown in Fig. 10. This figure clearly shows that optimal friction performance is obtained in the range from 20 to 30 grooves/mm^2. As the deep honing grooves provide a pathway for flow, particularly at small film thicknesses, decreasing the density of grooves will effectively block the pressure-driven flow and reduce the shear-driven flow carried by the ring. Pressure-driven flow blockage alters the effective lubricant viscosity whereas the shear-driven flow changes the effective ring profile [2]. Thus, decreasing the groove density mainly increases the hydrodynamic pressure generated between the ring and the liner. On the contrary, increasing the groove density was found to lead to higher oil consumption [20].

3.5. Effect of groove balance

The balance of the two sets of grooves and the honing angle are the most important properties of the honing texture [19]. During

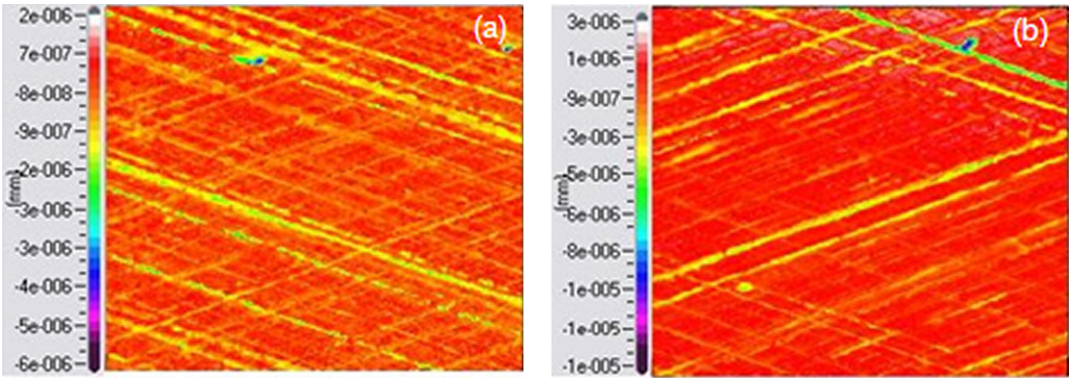

Fig. 11. (a) Balanced grooves (conform surface) and (b) unbalanced grooves (not conform surface).

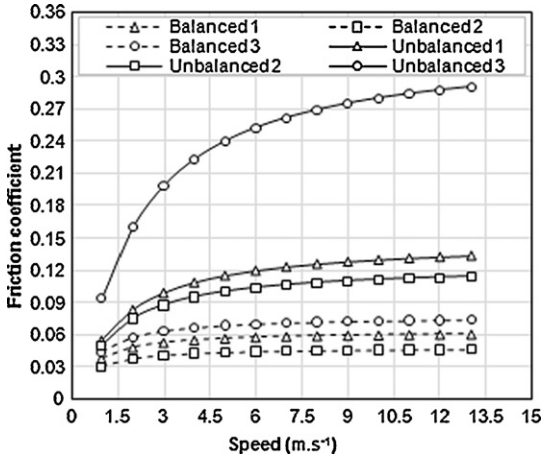

Fig. 12. Friction coefficients for different honed surfaces.

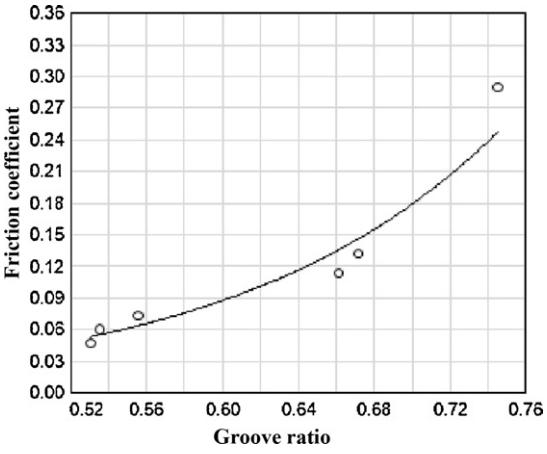

Fig. 13. Coefficient of friction vs groove ratio "R_g".

the industrial production of a honed-cylinder engine, it is also rated by visual inspection of fax-film images. Fig. 11 shows an example of balanced and unbalanced grooves in a plateau-honed surface. Experts opine that this feature mainly affects oil distribution and consumption.

Friction was predicted for three unbalanced groove surfaces and three balanced grooves surfaces for various contact sliding

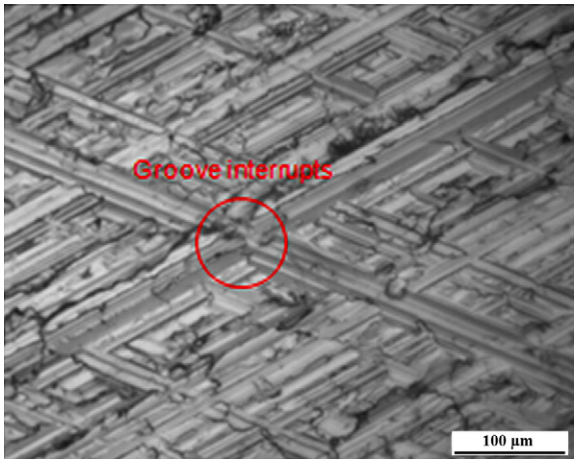

Fig. 14. Honing textures presenting an interrupted groove.

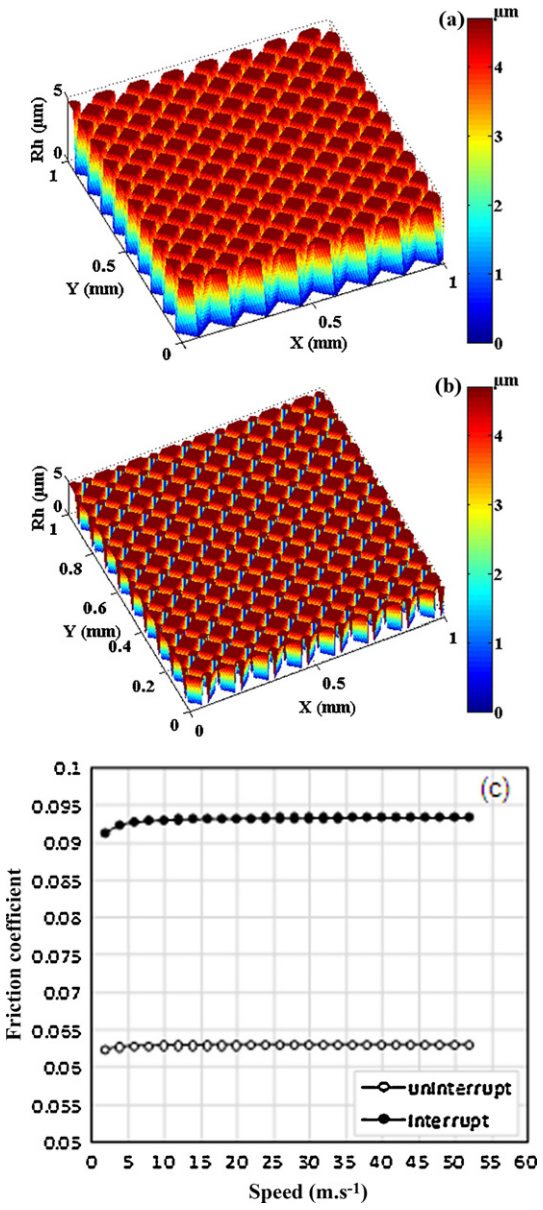

Fig. 15. Groove interrupts effect on friction: (a) honed surface with continuous grooves, (b) honed surface with discontinuous grooves, and (c) friction coefficient prediction.

velocities. Fig. 12 shows the friction coefficient prediction for six surfaces versus velocity. The unbalanced groove surfaces show a higher friction coefficient than the balanced one. The balance of grooves clearly affects the friction performance. In fact, the asymmetrical distribution of grooves leads to higher friction loss.

The friction coefficient versus groove ratio parameters can be plotted for $12\,m\,s^{-1}$ as in Fig. 13. The friction coefficient growth exponentially appears with the honing ratio parameter R_g. The lower friction can be obtained for the perfect balanced grooves ($R_g = 0.5$). Thus, this parameter becomes very significant for surface quality inspection and engine performance.

3.6. *Effect of groove interrupts*

Another aspect which could affect friction is the continuity of the grooves. It is considered a background texture including all

deviations from an "ideal" groove texture" like chatter marks, holes, flakes and material smearing, etc. [4,24]. In Fig. 14, a groove interrupt is marked in grey level image of real honed surface. Some automotive manufactures presume that groove interrupts are most important for oil consumption and noxious emissions.

The influence of groove continuities on engine behavior is not well known, probably because it is difficult to assess and quantify this background groove property by the objective and automated inspection method. Two synthesized honed surfaces respectively, with continuously (Fig. 15a) and interrupted (Fig. 15b) grooves, were generated and used in the numerical simulation. Fig. 15c, which represents the friction coefficient versus velocity for interrupted and uninterrupted grooves, shows that the friction coefficient increases by almost 50% when the grooves are discontinuous.

These discontinuities considerably affect the coefficient of friction and thus the engine behavior and noxious emission. Therefore, this background groove characteristic must be considered seriously in surface inspection criteria.

4. Conclusion

A prediction friction model in the hydrodynamic contact regime between the ring and cylinder liner was developed, taking into account the real topography of the cylinder liner. The properties of groove texture are generally related to the oil consumption. However, the friction performance in the piston ring/cylinder liner contact is associated with the plateau formation. Piston ring-pack friction reduction strategies through the cylinder liner groove texture optimization were analyzed. In this study, the groove texture (grooves balance, honing angle, etc.) have been demonstrated to greatly affect friction performance.

According the conclusions drawn from this work, some optimal groove texture characteristics have been proposed to reduce friction. They essentially include:

Groove balance in the range of [40–55°] or [115–130°];
Balanced and continuous grooves;
Grooves wide greater than 20 μm;
Groove density greater than 20 grooves/mm^2.

These results obtained are general and can potentially be applied to any reciprocating engine. Also, an additional friction reduction can be achieved by optimizing the surface roughness. An optimal amplitude ratio between the plateau roughness and valley depth must be determined. Finally, both oil consumption and ring-pack failure through scuffing are complex phenomena rather difficult to predict numerically. Engine testing, then will allow the verification of this optimal spatial morphology and will also permit the quantification of the effects of the proposed liner groove texture characteristics on oil consumption and scuffing tendency.

Acknowledgement

The authors thank S. Legros for his dedication and computer support during this work.

References

[1] Jocsak J, Wong VW, Tomanik E, Tian T, Lemke H. The characterization and simulation of cylinder liner surface finishes. In: Proceedings of the spring technical conference of the ASME Internal Combustion Engine Division, Art. No. ICES2005-1080. 2005. p. 457–67.
[2] Jocsak J, Wong V, Tian T. The effects of cylinder liner finish on piston ring pack friction. In: Proceedings of the 2004 Fall technical conference of the ASME Internal Combustion Engine Division, vol. 84. 2004. p. 1–849.
[3] Malburg MC, Raja J. Characterization of surface texture generated by plateau honing process. CIRP Ann 1993;42:637–9.
[4] Mainsah E, Greenwood JA, Chetwynd DG. Metrology and properties of engineering surfaces, vol. 24. Kluwer Academic Publishers; 2001 p. 3–276.
[5] Srivastava DK, Agarwal AK, Kumar J. Effect of liner surface properties on wear and friction in a non-firing engine simulator. Mater Des 2007;28:1632–40.
[6] Etsion I. State of the art in laser surface texturing. J Tribol 2005;127:248–53.
[7] Ryk G, Etsion I. Testing piston rings with partial laser surface texturing for friction reduction. Wear 2006;261:792–6.
[8] Lu X, Khonsari MM. An experimental investigation of dimple effect on the Stribeck curve of journal bearings. Tribol Lett 2007;27:169–76.
[9] Krupka I, Hartl M. The effect of surface texturing on thin EDH lubrication film. Tribol Int 2007;40:1100–10.
[10] Kovalchenko A, Ajayi O, Erdemir A, Fenske G, Etsion I. The effect of laser surface texturing on transitions in lubrication regimes during unidirectional sliding contact. Tribol Int 2005;38:219–25.
[11] Costa HL, Hutchings IM. Hydrodynamic lubrication of textured steel surfaces under reciprocating sliding conditions. Tribol Int 2007;40:1227–38.
[12] Tomanik E. Friction and wear bench tests of different engine liner surface finishes. Tribol Int 2008;41:1031–8.
[13] Ren N, Nanbu T, Yasuda Y, Zhu D, Wang Q. Micro textures in concentrated-conformal-contact lubrication: effect of distribution patterns. Tribol Lett 2007;28:275–85.
[14] Nanbu T, Ren N, Yasuda Y, Zhu D, Wang Q. Micro textures in concentrated-conformal-contact lubrication: effects of texture bottom shape and surface relative motion. Tribol Lett 2008;29:241–52.
[15] Caciu C, Decencière E. Numerical analysis of a 3D hydrodynamic contact. Int J Numer Meth Fluids 2006;51:1355–77.
[16] Caciu C. Analyse et optimisation des surfaces des chemises de moteurs thermiques. PhD thesis. École des Mines de Paris; 2006 [in French].
[17] Habchi W, Demirci I, Eyheramenndy D, Morales-Espejel G, Vergne P. A finite element approach of thin film lubrication in circular EHD contacts. Tribol Int 2007;40:1466–73.
[18] Caciu C, Decencière E, Jeulin D. Numerical analysis of the consequences of roughness modifications in 3D hydrodynamic contacts. Tribol Trans 2008;51:483–93.
[19] Krahe D, Beyerer J. A parametric method to quantify the balance of groove sets of honed cylinder bores. In: Proceedings of SPIE – The International Society for Optical Engineering. 1997. p. 192–201.
[20] Sabri L, Mezghani S, El Mansori M, Le-Lan JV. Toward an objective 3D description for quality assessment of manufactured honed surfaces. Trans N Am Manuf Res Inst SME Greenville, USA 2009;3:661–8.
[21] Puente Leon F. Evaluation of honed cylinder bores. CIRP Ann 2002;51(1):503–6.
[22] Jocsak J, Li Y, Victor TT, Wong W. Analyzing the effects of three-dimensional cylinder liner surface texture on ring-pack performance with a focus on honing groove cross-hatch angle. In: Proceedings of the Fall technical conference of the ASME Internal Combustion Engine Division. 2005.
[23] Anderberga C, Pawlus P, Rosen BG, Thomas TR. Alternative descriptions of roughness for cylinder liner production. J Mater Process Technol 2009;209:1936–42.
[24] De Chiffre L, Lonardo P, Trumpold H, Lucca DA, Goch G, Brown CA, et al. Quantitative characterization of surface texture. CIRP Ann 2000;49(2):635–50.